UNIVERSITY OF SUSSEX

DOCTORAL THESIS

Optimisation studies and background estimation in searches for the supersymmetric partner of the top quark in all-hadronic final states with the ATLAS Detector at the LHC

A thesis submitted in fulfillment of the requirements for the degree of Doctor of Philosophy

in the

Experimental Particle Physics Research Group
School of Mathematical and Physical Sciences

Author:
Fabrizio MIANO

Supervisor:
Dr. Fabrizio SALVATORE

11th October 2017

Dedicated to my family.

Have no fear for atomic energy
'cause none of them can stop the time

Robert Nesta Marley

Acknowledgments

Thanks to every single thing that went wrong. It made me stronger.

Declaration

I, Fabrizio MIANO, hereby declare that this thesis, titled, "Optimisation studies and background estimation in searches for the supersymmetric partner of the top quark in all-hadronic final states with the ATLAS Detector at the LHC" has not been and will not be, submitted in whole or in part to another University for the award of any other degree.

Brighton, June 2018

Fabrizio MIANO

University of Sussex
School of Mathematical and Physical Sciences
Experimental Particle Physics Research Group

Doctoral Thesis

Optimisation studies and background estimation in searches for the supersymmetric partner of the top quark in all-hadronic final states with the ATLAS Detector at the LHC

---

by Fabrizio MIANO

Abstract

This thesis presents searches for supersymmetry in $\sqrt{s} = 13$ TeV proton-proton collisions at the LHC using data collected by the ATLAS detector in 2015, 2016 and 2017. Events with 4 or more jets and missing transverse energy were selected. Kinematic variables were investigated and optimisations were performed to increase the sensitivity to supersymmetric signals. Standard Model backgrounds were estimated by means of Monte Carlo simulations and data-driven techniques. Before analysing the data in the blinded signal regions the agreement between data and background predictions and the extrapolations from control and validation regions to signal regions were validated. The analysis yielded no significant excess in any of the analyses performed. Therefore limits were set and the results were interpreted as lower bounds on the masses of supersymmetric particles in various scenarios and models.

Contents

List of Tables

List of Figures

Introduction

Last thing to write

Chapter 1

The Standard Model, Supersymmetry, and the motivations behind it

A theory is something nobody believes, except the person who made it. An experiment is something everybody believes, except the person who made it.

Albert Einstein

The Standard Model (SM) of particle physics is an effective theory that aims to provide a general description of fundamental particles and the phenomena we see in nature, i. e. the way they interact. Unfortunately, our understanding of nature is still limited due to some opened question to which the SM is not able to answer to, yet.

In this chapter, an overview of the SM will be presented in Section 1.1 together with the limitations of such theory and some of the reasons behind the need of an extension. For the last decades theoretical physicsts have been trying to provide extensions to the SM, the so-called beyond-the-SM theories. Among these, one of the most popular, Supersymmetry which will be discussed in Section 1.2.

1.1 The Standard Model

The 20^{th} century can be considered a quantum revolution. Several experiments led to discoveries which were found to be, together with the formalised theory, a solid base of the Standard Model of particle physics and our description of nature. Several particles were predicted first by the SM and then experimentally observed e. g. the W and the Z bosons, the τ lepton, [4], and more recently the Higgs boson at the LHC discovered by ATLAS [5] and CMS [6].

The SM lays on a Quantum Field Theory (QFT) where particles are treated like fields. It can describe three of the four fundamental forces; weak, electromagnetic, and strong. As of today, gravity is not considered in the SM. Sections 1.1.1 and 1.1.2 will be focused on the description of the fields together with the carriers of the information, and on the limitations that such theory implies, respectively.

1.1.1 Overview

The most general classification of the particles within the SM can be made by means of spin. Fermions have half-integer spin values - and are usually referred to as matter -, and bosons have integer-spin values. A noteworthy subset of bosons is formed by the Spin-1 bosons (also known as gauge bosons). These can be considered the information carriers or, in fact, the mediators of the forces.

Fermions

Six quarks and six leptons belong to the fermions family. The six quarks of the SM can be grouped into doublets of three generations. There are three generations, each containing four particles; one charged lepton, one neutrino, and one up- and down-type quark. The masses of the charged leptons and quarks increase with the generation.

$$\begin{pmatrix} u \\ d \end{pmatrix}, \quad \begin{pmatrix} c \\ s \end{pmatrix}, \quad \begin{pmatrix} t \\ b \end{pmatrix}$$

The up-type quarks (up, charm, top) have charge $+\frac{2}{3}e$ and the down-type quarks (down, strange, beauty/bottom) have charge $-\frac{1}{3}e$, where e is the electron charge. Quarks also have another quantum number that can be seen as the analogue of the electric charge, the colour charge. There are three different states of the colour charge; "red", "green" and "blue". Three of the six leptons $(e\,,\mu\,,\tau)$ are electrically charged and three of them electrically neutral $(\nu_e\,,\nu_\mu\,,\nu_\tau)$ and, as quarks they can also grouped into generations:

$$\begin{pmatrix} \nu_e \\ e^- \end{pmatrix}, \quad \begin{pmatrix} \nu_\mu \\ \mu^- \end{pmatrix}, \quad \begin{pmatrix} \nu_\tau \\ \tau^- \end{pmatrix}$$

Forces of Nature

1.1.2 Limitations of the Standard Model

1.2 Supersymmetry

1.2.1 Why SUSY?

1.2.2 Minimal Supersymmetric Standard Model

1.2.3 *R*-parity SUSY

1.2.4 Simplified models

1.2.5 Phenomenological MSSM

Chapter 2

The ATLAS Experiment at the LHC

ATLAS (A Toroidal LHC ApparatuS) is one of the four main experiments (ATLAS, CMS, ALICE, LHCb) taking data at a center-of-mass energy of 13 TeV using beams delivered by the Large Hadron Collider (LHC). In this chapter an overview of the LHC will be given in Section 2.1, then the ATLAS detector will be described in Section 2.2, and finally the Trigger system, used to cleverly store the data, will be described in Section 2.3. A more in-depth description of the Trigger algorithms I have been involved in will be given in Chapter 3.

2.1 The LHC

As of today, the LHC is the worlds largest and most powerful particle accelerator. It was designed to help answer some of the fundamental open questions in particle physics by colliding protons at an unprecedented energy and luminosity. It is located at the European Organisation for Nuclear Research (CERN), in the Geneva area, at a depth ranging from 50 to 175 metres underground. It consists of a 27-kilometre ring made of superconducting magnets, and inside it two high-energy particle beams travel in opposite directions and in separate beam pipes.

The beams are guided around the ring by a strong magnetic field generated by coils - made of special electric cables - that can operate in a superconducting regime.1232 superconducting dipole and 392 quadrupole magnets, with an average magnetic field of 8.3 T, are employed and kept at a temperature below 1.7 K, in order to preserve their superconducting properties. The formers are used to bend the beams and the latters to keep them focused while they get accelerated.

The collider first went live on September 2008 even though, due to a magnet quench incident that damaged over 50 superconducting magnets, it has been operational since November 2009 when low-energy beams circulated in the tunnel for the first time since the incident. This also marked the start of the main research programme and the beginning of the so-called Run 1: first operational run (2009 - 2013).

Performance of the LHC

In June 2015 the LHC restarted delivering physics data, after a two-year break, the so-called Long Shutdown 1 (LS1), during which the magnets were upgraded to handle the current required to circulate 7-TeV beams. It was the beginning of the so-called Run 2 - second operational run (2015-2018) - during which LHC has collided up to 10^{11} bunches of protons every 25 ns at the design luminosity - the highest luminosiy the detector was designed to cope with - of $2 \cdot 10^{34}\mathrm{cm}^{-2}\mathrm{s}^{-1}$. The definiton of the luminosity is:

$$\mathcal{L} = f\frac{n_b N_1 N_2}{4\pi\sigma_x\sigma_y} \tag{2.1}$$

where N_1 and N_2 are the number of protons per bunch in each of the colliding beams, f is the revolution frequency of the bunch collisions, n_b the number of proton per bunch, and σ_x and σ_y are the horizontal and vertical dimensions of the beam. The luminosity is strictly related to the number of collisions occurring during a certain experiment via the following:

$$\mathcal{N}_{\mathrm{event}} = \mathcal{L}\sigma_{\mathrm{event}} \tag{2.2}$$

where σ_{event} is the cross section of the process under investigation. It has not only collided protons but also heavy ions, in particular lead nuclei at $\sqrt{s_{NN}} = 5.02$ TeV, at a luminosity of $10^{27}\mathrm{cm}^{-2}\mathrm{s}^{-1}$[7].

Acceleration stages

Before reaching the maximum energy, the proton beams are accelerated by smaller accelerators through various stages. Figure 2.1 shows a sketch of the CERN's accelerator complex. It all begins at the linear accelerator LINAC 2. Here protons are accelerated up to 50 MeV, and then injected in the Proton Synchrotron Booster (PSB) where they reach 1.4 GeV. The next stage is the Proton Synchrotron (PS), which boosts the beams up to 25 GeV and then the Super Proton Synchrotron (SPS) makes them reach energies up to 450 GeV. Eventually, the beams are injected in bunches with a 25 ns spacing into the LHC, where they travel in opposite directions, while they are accelerated to up to 13 TeV. Once

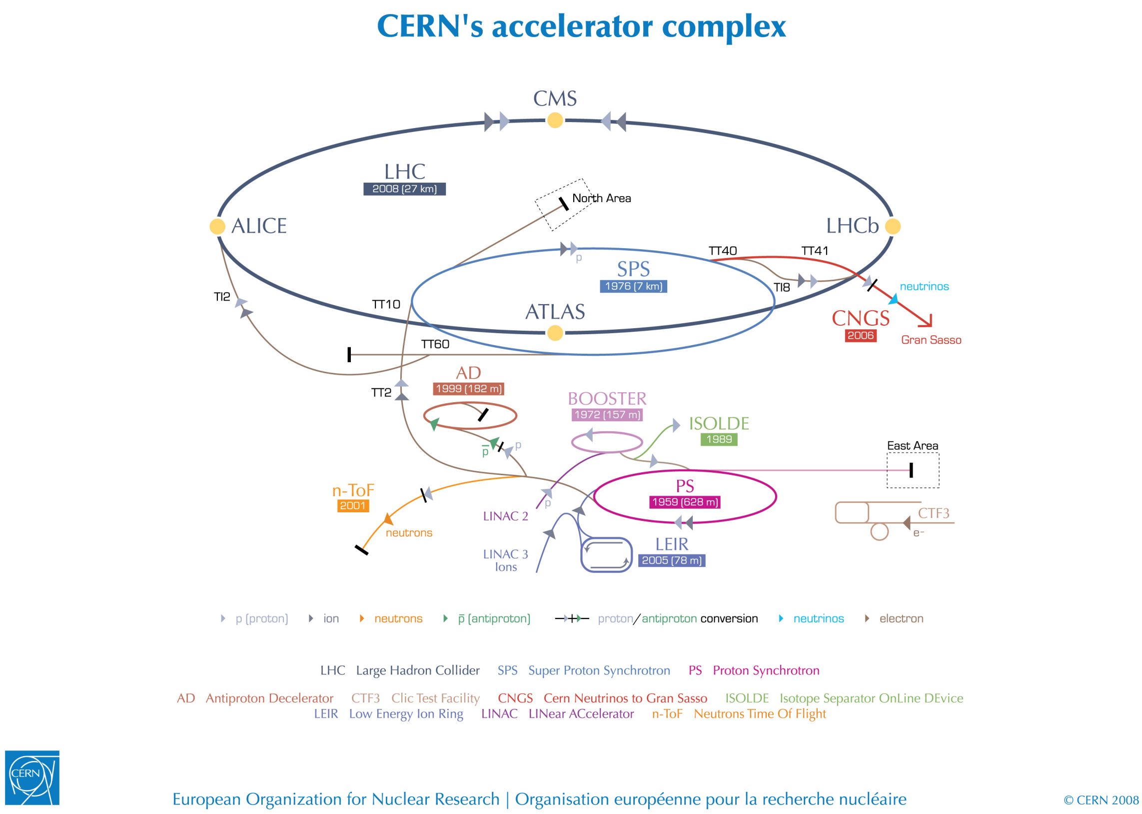

Figure 2.1: CERN Accelerator complex. The LHC is the last ring (dark grey line). Smaller machines are used for early-stage acceleration and also to provide beams for other experiments [1].

the bunches reach the maximum energy, they are made collide at four different points, inside four experiments around the ring [8].

The heavy ion beams acceleration procedure is slightly different. Their journey starts at LINAC 3 first, and the Low Energy Ion Ring (LEIR) then, before they make their way into the PS where they follow the same path as the protons [8].

The four large detectors on the collision points are; the multi-purpose detectors A Toroidal LHC ApparatuS (ATLAS), and Compact Muon Solenoid (CMS) [9], Large Hadron Collider beauty (LHCb) [10], which focuses on flavour physics, and A Large Ion Collider Experiment (ALICE) [11] which specialises in heavy ion physics. The *big four* are not the only experiments at the CERN's accelerator complex. There also are smaller experiments based at the the four caverns about the collision points e.g. TOTEM, LHCf and MoEDAL, but this will not be discussed any further in this thesis.

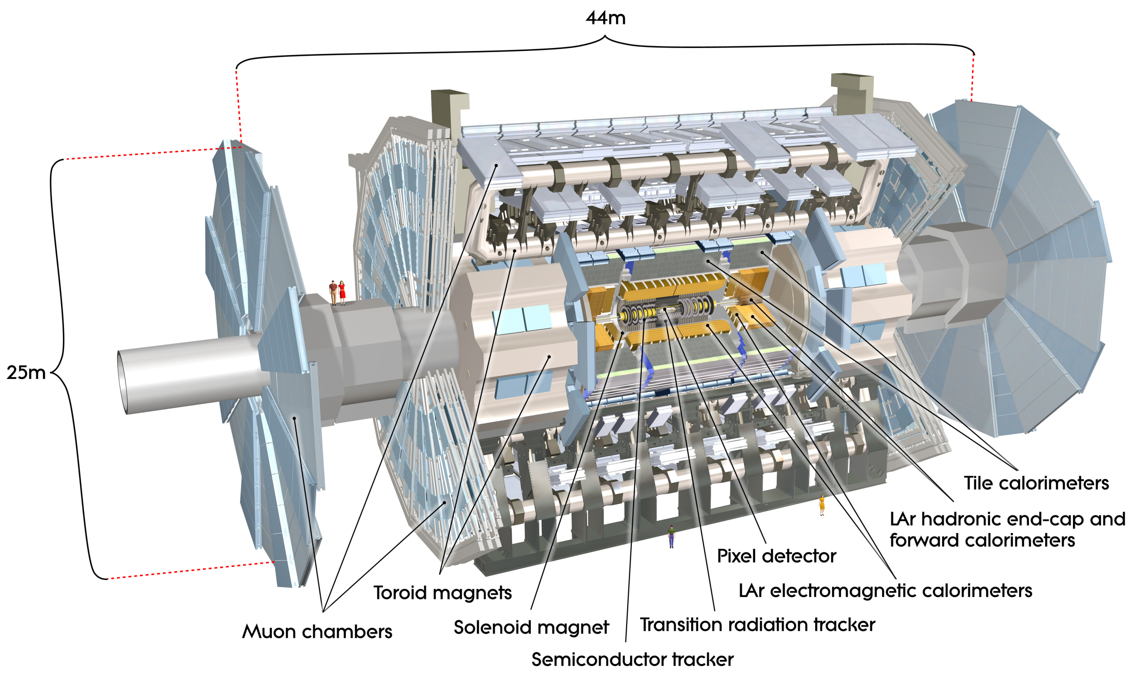

Figure 2.2: Cut-away view of the ATLAS detector. The dimensions of the detector are 25 m in height and 44 m in length. The overall weight of the detector is approximately 7000 tonnes [1].

2.2 The ATLAS Detector

ATLAS is a general-purpose detector designed to collect data with the highest luminosity provided by the LHC. It is located at CERN's Point 1 cavern and it measures about 45 m in length and 25 m in diameter. It has a forward-backward symmetric cylindrical geometry with respect to the interaction point and it is designed to reconstruct and measure physics objects such as elctrons, muons, photons and hadronic jets. Its design was optimised to be as sensitive as possitble to the discovery of the Higgs boson and beyond-the-Standard-Model (BSM) physics. In fact, thanks to the other sub-systems, ATLAS is able to observe all possible decay products by covering nearly 4π steradians of solid angle.

In Figure 2.2 a cut-away view of ATLAS with all its components is shown. The inner-most layer is the Inner Detector (ID) which is the core of the tracking system and consists of a Pixel, a Silicon micro-strip tracker (SCT), and a Transition Radiation Tracker (TRT). It is submerged in a 2 T magnetic field, generated by a thin superconducting solenoid, which bends all the charged particles' trajectories allowing transverse momemtum measurement. The electromagnetic and hadronic calorimeters form the next layer and they are both used to perform precise energy measurements of photons, electrons, and hadronic jets. Finally, the outermost layer corresponds to the Muon Spectrometer (MS) which, together with the ID, enclosed in a toroidal magnetic field, allows precise measurement of momentum and position of muons. These sub-detectors will be discussed in more detail in the following sections.

The ATLAS coordinate system

A coordinate system is taken on for the spatial definition of the sub-systems and kinematic measurement of physics processes. Such system is defined starting from the interaction point, defined as the origin. The z-axis is defined by the beam direction and the $x - y$ plan, as transverse to the beam direction.

A quantity, known as pseudorapidity, (η), is defined to describe the angle of a particle coming out of the collision, with respect to the beam axis:

$$\eta \equiv -\ln(\tan(\theta/2))$$

Here θ is the polar angle. The azimuthal angle, ϕ, is defined around the beam axis and the polar angle. In the (η, ϕ) space a distance ΔR can be therefore defined as

$$\Delta R = \sqrt{\Delta\eta^2 + \Delta\phi^2}$$

where $\Delta\eta$ and $\Delta\phi$ are the differences in pseudorapidity and azimuthal angle between any two considered objects. A central and a forward region of pseudorapidity are also defined such that the detector components are described as part of the *barrel* if they belong to the former or as part of the *end-caps* if they belong to the latter.

2.2.1 The Magnet System

The ATLAS magnet system, 26 m long with a 22 m diameter, generates the magnetic field needed to bend the trajectories of charged particles in order to perform momentum measurement. Figure 2.3a and 2.3b show the geometry of the system and its components, which are made of NbTi - superconducting material - and will be described in the following parahraphs.

The Central Solenoid

With an axial length of 5.8 m, an inner radius of 2.46 m, and an outer radius of 2.56 m, the central solenoid magnet is located between the ID and the ECAL. Its function is to bend

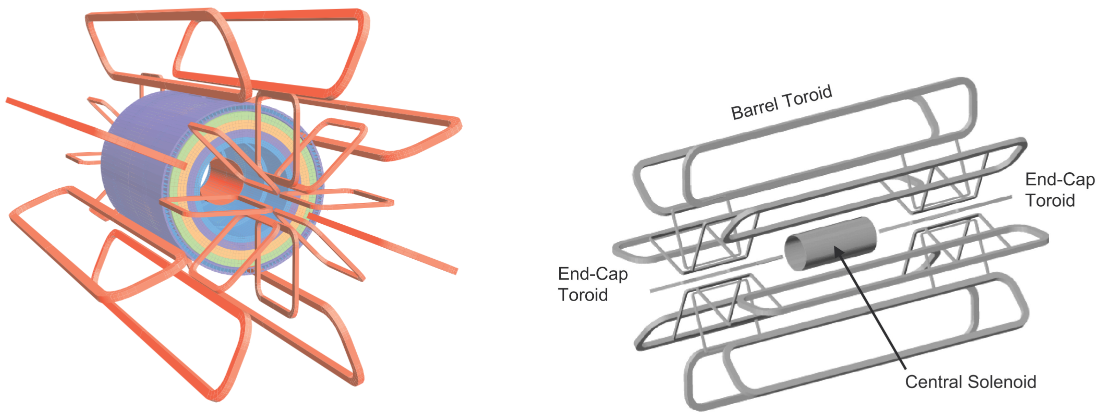

(a) Geometry of magnet windings and tile calorimeter steel. The eight barrel toroid coils, with the end-cap coils interleaved are visible. The solenoid winding lies inside the calorimeter volume [2].

(b) Schematic view of the superconducting magnets [12].

Figure 2.3: The ATLAS magnet system.

the charged particles that go through the ID and it is aligned on the beam axis providing a 2 T axial magnetic field that allows accurate momentum measurement up to 100 GeV [12].

The Barrel and the End-cap Toroids

Figure 2.3b displays the toroid magnetic system that surrounds the calorimeters. With its cylindrical shape this component consists of a barrel and two end-caps toroids, each with eight superconducting coils. The system allows accurate measurement of muon momenta using a magnetic field of approximately 0.5 T (barrel) for the central regions and 1 T (end-cap) for the end-cap regions, respectively, which bends the particles in the θ direction.

2.2.2 The Inner Detector

The Inner Detector (ID) [13] is the innermost component of the ATLAS detector i. e. the nearest sub-detector to the interaction region and it is used to reconstruct charged particle tracks used in the selection of physics objects. In fact, it allows robust track reconstruction, with accurate impact parameter resolution ($\sim 20 \mu m$) and precise primary and secondary vertex reconstruction for charged particles (tracks) above 500 MeV and within $|\eta| < 2.5$.

The ID is comprised of independent and concentric sub-systems, which are all shown

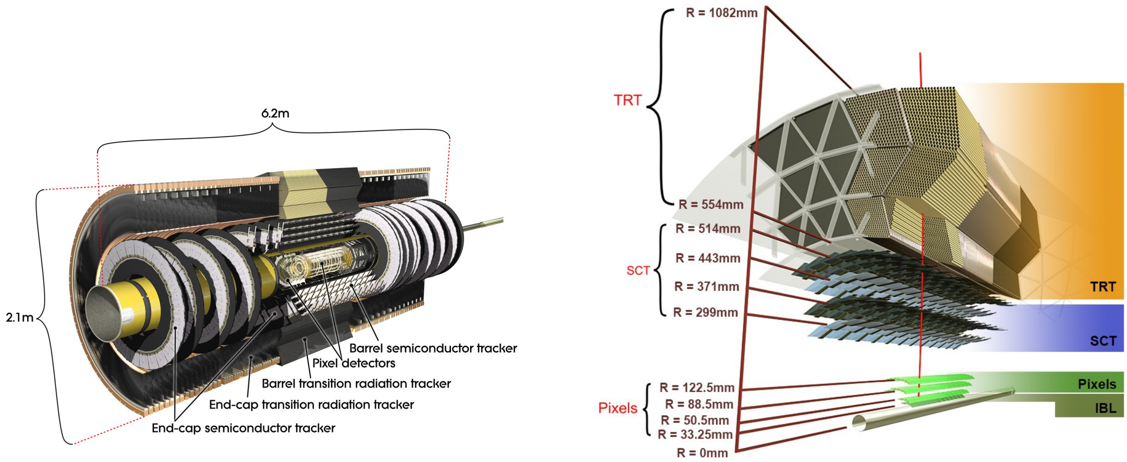

(a) Overview of the ATLAS ID with labels and dimensions.

(b) Diagram of the ATLAS ID and its sub-detectors.

Figure 2.4: The ATLAS Inner Detector

in Figure 2.4:

- Insertable B-Layer (IBL):
  innermost Pixel Detector layer added during ATLAS Run-2 upgrade (2013/2014) to improve vertexing and impact parameter reconstruction;

- Silicon Pixel Tracker (Pixel):
  made of silicon pixel layers and used mainly for reconstructing both the primary and secondary vertices in an event;

- SemiConductor Tracker (SCT):
  comprised of silicon microstrip layers; thanks to its resolution ($17 \times 580\,\mu$m) it can accurately measure particle momenta;

- Transition Radiation Tracker (TRT):
  final layer comprised of various layers of gaseous straw tube elements surrounded by transition radiation material.

These sub-detectors will be discussed in the following sections.

IBL

The IBL [14] is the innermost Pixel Detector layer as shown in Figure 2.4b. It is comprised of 6M channels and each pixel measures $50 \times 250\,\mu$m. Its resolution is $8 \times 40\,\mu$m,The addition of this new layer brought a considerable improvement on the performance of the

Pixel Detector by enhancing the quality of impact parameter reconstruction of tracks. In particular, this was achieved by improving the vertex finding efficiency and the tagging of bottom-quark-initiated jets (b-jets) which, in case of a B-layer failure, can be restored by the IBL. Besides these improvements, the IBL insertion allowed ATLAS to better cope with high luminosity effects such as the increase in event pile-up, which leads to high occupancy and read-out inefficiency.

Pixel

The Pixel detector is comprised of 1750 identical sensorchip-hybrid modules, each covering an active area of 16.4×60.8 mm. The total number of modules correspond to roughly 80 million semiconductor silicon pixels. The nominal pixel size is 50 μm in the ϕ direction and 400 μm in the barrel region, along the z-axis (beam axis) [15]. The reason why such a large amount of pixels is employed is justified by the need to cope with the high luminosity in ATLAS. The silicon pixel detector measures 48.4 cm in diameter and 6.2 m in length providing a pseudorapidity coverage of $|\eta| < 2.5$. Figure 2.4b shows the three concentric barrel layers placed at 50.5 mm, 88.5 mm and 122.5 mm respectively. Furthermore, the Pixel detector is made of six disk layers, three for each forward region, such that when a charged particle crosses the layers it will generate a signal at least in three space points. The fine granularity of such detector allows accurate measurement and precise vertex reconstruction, as it provides a more accurate position measurement as a large detection area is available. In particular, it has a resolution of $10 \times 115\,\mu$m.

SCT

The SCT is made of 4088 modules of silicon micro-strip detectors arranged in four concentric barrel layers. It is mainly used for precise momentum reconstruction over a range $|\eta| < 2.5$ and it was designed for precision measurement of the position using four points (corresponding to eight silicon layers), obtained as track hits when crossing the layers. Figure 2.4b shows the structure of the SCT with its four concentric barrel layers with radii ranging from 299 mm to 514 mm and two end-cap layers. Each module has an intrinsic resolution of 17 μm in the $R - \phi$ direction and 580 μm in the z direction. As the SCT is further away from the beam-pipe than the Pixel detector, it has to cope with reduced particle density. This allows for reduced granularity mantaining the same level of performance of the Pixel detector: SCT can use ~ 6.3 million read-out channels.

TRT

The last and outermost of the sub-systems in the ID is the TRT. It is a gaseous detector which consists of 4 mm diameter straw tubes wound from a multilayer film reinforced with carbon fibers and containing a 30 μm gold plated tungsten wire in the center. The straw is filled with a gas mixture of 70% Xe, 27% CO_2 and 3% O_2 [16]. As shown in Figure 2.4b, its section consists of three concentric layers with radii ranging from 544 mm to 1082 mm, each of which has 32 modules containing approximately 50,000 straws, 1.44 m in length, aligned parallel to the beam direction with independent read-out at both ends. Both end-cap sections are divided into 14 wheels, with roughly 320,000 straws in the R-direction. The average 36 hits per track in the central region of the TRT allow continuous tracking to enhance pattern recognition and momentum resolution in the $|\eta| < 2.5$ region. It also improves the p_{T} resolution for longer tracks.

2.2.3 The Calorimeters

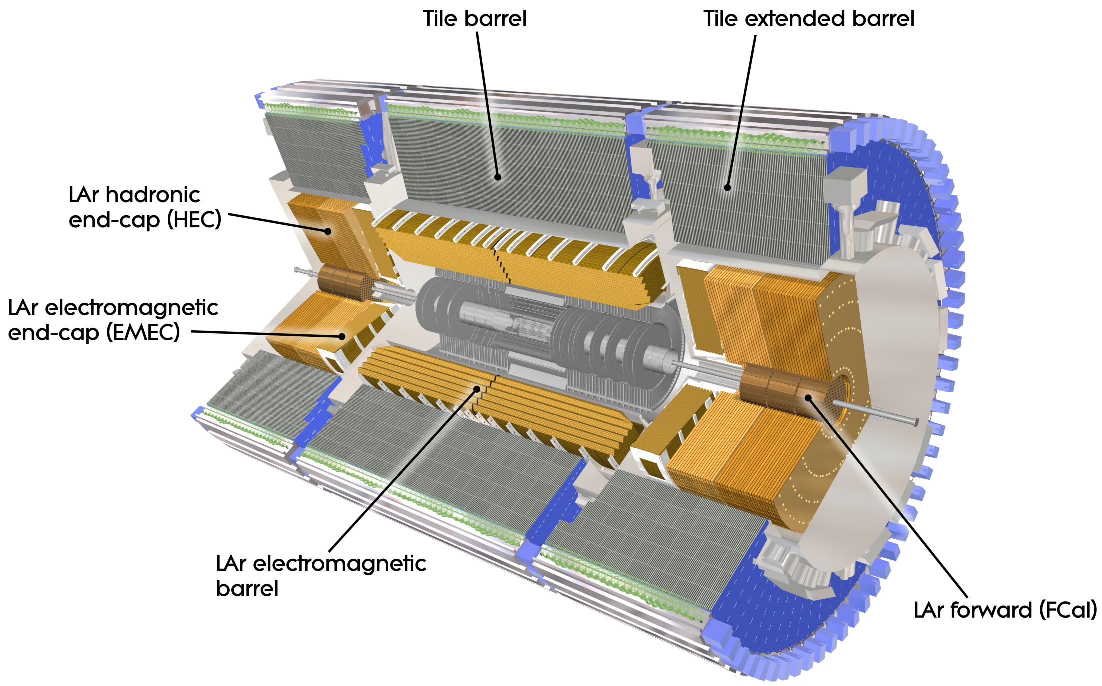

Figure 2.5: A computer generated image of the full calorimeter.

The ATLAS Calorimeter system, shown in Figure 2.5, is comprised of two main sub-systems; the electromagnetic calorimeter (ECAL) and hadronic calorimeter (HCAL), which are designed to stop and measure the energy of electromagnetic-interacting and hadronic particles respectively. The combination of the two provides full coverage in ϕ and $|\eta| < 4.95$. Particles slow down and lose energy generating showers when crossing different layers.

The ECAL is comprised of one barrel and two end-cap sectors employing liquid Argon (LAr). The showers hereby develop as electrons pairs which are then collected.

The HCAL is also comprised of one barrel and two end-cap sectors. The sensors in the barrel of the HCAL are tiles of scintillating plastic whereas LAr is employed for the end-cap.

A forward region, the closest possible to the beam, is covered by a LAr forward calorimeter (FCal).

The LAr and Tile Calorimeter will be briefly discussed in the following parapgraphs.

The Liquid Argon Calorimeters

The ECAL is comprised of multiple layers of liquid Argon (LAr) sampler and lead absorber. The choice of its accordion-geometry design brought two main advantages; full ϕ coverage with no non-interactive regions (no cracks); fast extraction of signals coming from both front or rear end of the electrodes. It is made of two half-barrel wheels, both placed in the barrel cryostat, that provide a pseudorapidity coverage up to $|\eta| < 1.475$ and two end-cap detectors providing $1.375 \leq |\eta| \leq 3.20$ coverage in two end-cap cryostats. The junction between the barrel and end cap components defines the crack region and any signal coming from the crack region is therefore discarded.

In the $|\eta| < 1.8$ region there is an additional layer, placed at the front of the calorimeter, that is made of a thin (0.5 cm in the end-cap and 1.1 cm in the barrel) LAr layer with no absorber [17]. This additional layer was designed to correct for the energy lost, as particles enter the calorimeter, by taking a measurement just before the majority of the electomagnetic shower is developed.

The Tile calorimeter

The main purpose of the hadronic calorimeter is to measure the energy of hadronic showers. It is built employing steel and scintillating tiles coupled to optical fibres which are read out by photo-multipliers. As shown in Figure 2.5, the HCAL is made up of three cylinders; a central barrel, 5.64 m long covering a region $|\eta| < 1.0$, and two extended barrel, 2.91 m long covering a reigon $0.8 < |\eta| < 1.7$. Each cylinder is made up of 64 modules and each module is in turn made up of three layers. Ultimately, the smallest section of the calorimeter module is a cell with a $\Delta\phi \times \Delta\eta = 0.1 \times 0.1$ granularity for the two innermost layers and $\Delta\phi \times \Delta\eta = 0.2 \times 0.1$ for the outermost one.

2.2.4 The Muon Spectrometer

The MS [18], shown in Figure 2.6, is the outermost sub-system of the whole ATLAS detector. As such, it surrounds the calorimeters and its main function is to perform precision measurement of muons momenta. The deflection of muon tracks employing large superconducting air-core toroid magnets and high-precision tracking chambers is at the heart of such high precision measurement.

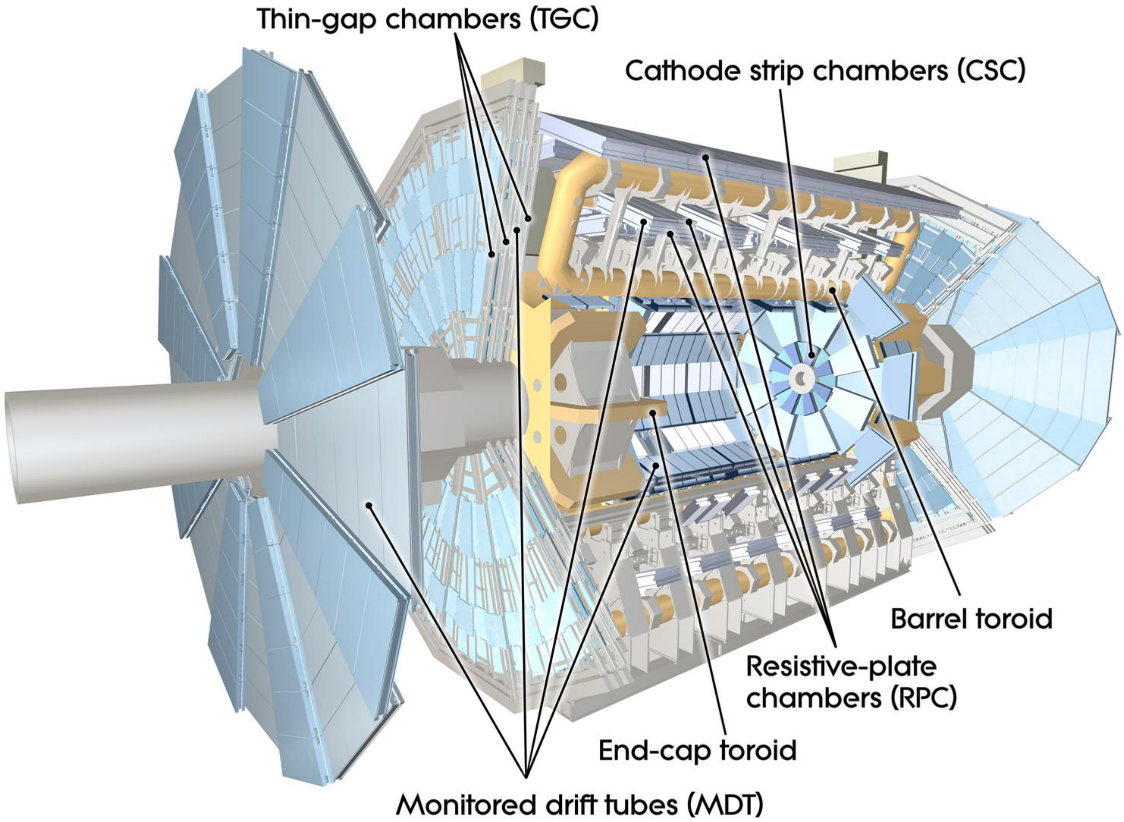

Figure 2.6: Cut-away view of the ATLAS muon system [2].

The MS is comprised of one large barrel toroid, covering the region $|\eta| \leq 1.4$, and two end-cap toroids, covering $1.6 < |\eta| \leq 2.7$ which are employed together to achieve the track-bending effect wanted. The magnitude of the magnetic field in the barrel, generated by eight large superconducting coils, ranges from 0.5 to 2 T.

Around the beam axis, three cylindrical layers make way for the chambers, placed in planes perpendicular to the beam, used to measure tracks.

Monitored Drift Chambers (MDTs) are employed over most of the pseudorapidity range to provide precision measurement of track coordinates in the bending direction. Cathode Strip Chambers (CSCs) are instead employed at large pseudorapidity ($2 < |\eta| < 2.7$). Finally, in the end-cap regions Thin-Gap Chambers (TGCs) together with Resistive-Plate Chambers (RPCs) are dedicated to the Trigger System discussed in Section 2.3.

2.3 The ATLAS Trigger System

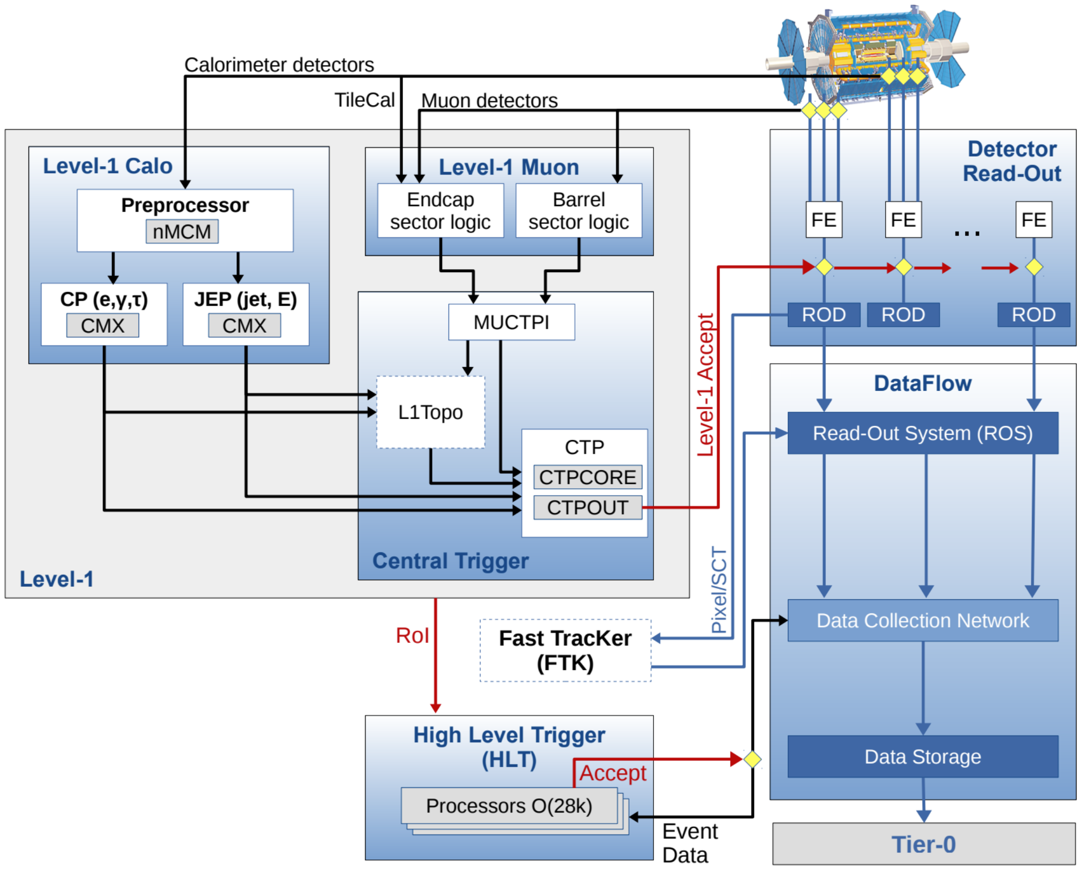

Figure 2.7: The ATLAS TDAQ system. L1Topo and FTK were being commissioned during 2015 and not used for the results shown in this thesis [3].

The ATLAS Trigger System is at the heart of data taking. It is an essential component of any nuclear or particle physics experiment since it is responsible for deciding whether or not to store an event for later study [3]. The ATLAS Trigger system is employed to reduce the event rate from ~ 40 MHz[1] bunch-crossing[2] to ~ 200 Hz which corresponds

[1]The LHC delivers beams with a bunch-spacing of 25 ns.

[2]The term bunch-crossing is hereby used when referring to a collision between two bunches of protons. Since only a certain fraction of the total momentum carried by each proton contributes to the collision, an average number of interactions per bunch-crossing, $\langle \mu \rangle$ is used.

to roughly 300 MB/s.

The Trigger and Data Acquisition (TDAQ) system shown in Figure 2.7 consists of a hardware-based first level trigger (L1) and a software-based high-level trigger (HLT). The L1 trigger decision is formed by the Central Trigger Processor (CTP), which receives inputs from the L1 calorimeter (L1Calo) and L1 muon (L1Muon) triggers. The first level (L1), which was designed to perform the first selection step, is a hardware-based system that uses information from the calorimeter and muon subdetectors. It also defines the so-called Regions of Interest (RoIs) within the detector to be investigated by the next level trigger, the HLT. Additionally, a Fast TracKer (FTK) system [19] (not yet installed) will provide global ID track reconstruction at the L1 trigger rate using lookup tables stored in custom associative memory chips for the pattern recognition. The FPGA-based track fitter will perform a fast linear fit and the tracks are made available to the HLT. This system will allow the use of tracks at much higher event rates in the HLT than is currently affordable using CPU systems. However, the upgrade of the ATLAS trigger will not be discussed any further.

In the next sections the L1 and HLT will be briefly described.

2.3.1 Level 1 Trigger

The Level 1 Trigger identifies Regions of Interest (RoIs)[3] and passes these to HLT which will perform further investigations. Furthermore, in order to decide whether or not the event processing will continue, L1 selection uses only information coming from some parts of the detector to keep the input rate to a maximum of 100 kHz. L1 is implemented in fast custom electronics to keep the latency[4] below 2.5 μs. Event data from other sub-sytstem are temporarily stored in memories whilst L1 decision is taken.

The L1 topological trigger (L1-Topo) [20] is feeded with energy and direction information, about the objects found by the L1 calorimeter and the muon trigger, which will be processed by dedicated algorithms implemented in its own FPGAs. However, due to the 100 kHz read-out rate, not all the information collected by L1-Topo will be sent to the HLT, but only part of it. In order to properly seed the RoI-guided HLT reconstruction, speficic objects in combination with the correct topological criteria must be employed.

[3] $\eta - \phi$ regions where event features have been fouind by the L1 selection process.

[4] Time needed by an electric signal to get to the front-end electronics.

2.3.2 High-Level Trigger

The HLT is used to reduce the output rate down to 1 kHz and it has a ∼200 ms average decision time. Events that pass L1 trigger are then processed by the HLT using finer-granularity calorimeter information, precision measurements from the MS and tracking information from the ID. The HLT reconstruction can be run within RoIs identified at L1 or a so-called full-scan on the full detector can be performed. The track reconstruction in the Inner Detector is an essential component of the trigger decision in the HLT and it will be discussed more in detail in Chapter 3

Chapter 3

The *b*-jet Trigger Signature in ATLAS

The qualification task

3.1 Trigger Efficiency

Chapter 4

Event Simulation and Reconstruction

4.1 Event Generation

4.1.1 Parton Distribution Functions (PDFs)

4.1.2 Matrix Element Calculation

4.1.3 Parton Showers

4.1.4 Hadronisation

4.2 Detector Simulation

4.3 Reconstruction

4.3.1 Pile-up in the Inner Detector

4.3.2 Tracks

4.3.3 Vertex

4.3.4 Electrons

4.3.5 Muons

4.3.6 Jets

4.3.7 Taus

4.3.8 Missing Transverse Energy

4.4 Object Selection

4.4.1 Baseline Leptons

4.4.2 Baseline Jets

Chapter 5

Stop Searches in all-hadronic final states

Chapter 6

Results and Statistical Intepretations

Appendix A

Appendix A

Appendix B

Appendix B

Bibliography

[1] C. Lefèvre, *The CERN accelerator complex*,. http://cds.cern.ch/record/1260465. ix, 7, 8

[2] ATLAS Collaboration, *The ATLAS experiment at the CERN Large Hadron Collider*, Journal of Instrumentation **3** no. 08, (2008) S08003. http://stacks.iop.org/1748-0221/3/i=08/a=S08003. ix, 10, 15

[3] A. Collaboration, *Performance of the ATLAS Trigger System in 2015*, Eur. Phys. J. **C77** (2017), arXiv:1611.09661 [hep-ex]. ix, 16

[4] M. Herrero, *The Standard Model*,. https://arxiv.org/abs/hep-ph/9812242. 3

[5] ATLAS Collaboration, *Observation of a New Particle in the Search for the Standard Model Higgs Boson with the ATLAS Detector at the LHC*, Phys.Lett. **B716** (2012), arXiv:1207.7214 [hep-ex]. 3

[6] CMS Collaboration, *Observation of a new boson at a mass of 125 GeV with the CMS experiment at the LHC*, Phys.Lett. **B716** (2012), arXiv:1207.7235 [hep-ex]. 3

[7] J.M. Jowett, M. Schaumann, R. Alemany, R. Bruce, M. Giovannozzi, P. Hermes, W. Hofle, M. Lamont, T. Mertens, S. Redaelli, J. Uythoven, J. Wenninger, *The 2015 Heavy-Ion Run of the LHC*,. http://accelconf.web.cern.ch/accelconf/ipac2016/papers/tupmw027.pdf. 6

[8] O. S. Brüuning, P. Collier, P. Lebrun, S. Myers, R. Ostojic, J. Poole and P. Proudlock, *LHC Design Report*,. https://cds.cern.ch/record/782076. 7

[9] CMS Collaboration, *The CMS experiment at the CERN LHC*, Journal of Instrumentation **3** no. 08, (2008) S08004. http://stacks.iop.org/1748-0221/3/i=08/a=S08004. 7

[10] LHCb Collaboration, et. al, *The LHCb Detector at the LHC*, JINST (2008). 7

[11] ALICE Collaboration, *The ALICE experiment at the CERN LHC*, Journal of Instrumentation **3** no. 08, (2008) S08002. http://stacks.iop.org/1748-0221/3/i=08/a=S08002. 7

[12] A. Yamamoto, Y. Makida, R. Ruber, Y. Doi, T. Haruyama, F. Haug, H. ten Kate, M. Kawai, T. Kondo, Y. Kondo, J. Metselaar, S. Mizumaki, G. Olesen, O. Pavlov, S. Ravat, E. Sbrissa, K. Tanaka, T. Taylor, and H. Yamaoka, *The ATLAS central solenoid*, Nuclear Instruments and Methods in Physics Research Section A: Accelerators, Spectrometers, Detectors and Associated Equipment **584** no. 1, (2008) 53 – 74. http://www.sciencedirect.com/science/article/pii/S0168900207020414. 10

[13] ATLAS Collaboration, *The ATLAS Inner Detector commissioning and calibration*, Eur. Phys. **JC70** , arXiv:1004.5293. 10

[14] ATLAS Collaboration, *ATLAS Insertable B-Layer Technical Design Report*,. https://cds.cern.ch/record/1291633. 11

[15] G. A. et al., *ATLAS pixel detector electronics and sensors*, Journal of Instrumentation **3** no. 07, (2008) P07007. http://stacks.iop.org/1748-0221/3/i=07/a=P07007. 12

[16] A. Bingl, *The ATLAS TRT and its Performance at LHC*, Journal of Physics: Conference Series **347** no. 1, (2012) 012025. http://iopscience.iop.org/article/10.1088/1742-6596/347/1/012025/meta. 13

[17] ATLAS Collaboration, *ATLAS liquid-argon calorimeter: Technical Design Report*,. https://cds.cern.ch/record/331061. 14

[18] ATLAS Collaboration, *ATLAS muon spectrometer: Technical design report*,. https://cds.cern.ch/record/331068. 15

[19] ATLAS Collaboration, *Fast TracKer (FTK) Technical Design Report*,. https://cds.cern.ch/record/1552953. 17

[20] E. Simoni, *The Topological Processor for the future ATLAS Level-1 Trigger: from design to commissioning*, arXiv:1406.4316. 17